Supporting Information

Mystery of Three Borides: Differential Metal-Boron Bonding Governing Superhard Structures

Paul J. Robinson,[†] Gaoxiang Liu,[‡] Sandra Ciborowski,[‡] Chalynette Martinez-Martinez,[‡] Juan R. Chamorro,[‡] Xinxing Zhang, [‡] Tyrel M. McQueen,[‡] Kit H. Bowen, *,[‡] and Anastassia N. Alexandrova*,[†,§]

[†] Department of Chemistry & Biochemistry, University of California, Los Angeles, Los Angeles, California 90095, United States
[‡] Department of Chemistry and Materials Science, Johns Hopkins University, 3400 N. Charles Street, Baltimore, Maryland 21218, United States
[§] California NanoSystems Institute, Los Angeles, California 90095, United States

*Corresponding authors: kbowen@jhu.edu ; ana@chem.ucla.edu

'TABLE OF CONTENTS

1. Methodology

a. Theoretical Methods

Cluster structures were optimized using CASPT2 (ReB_2), MRCI (TiB_2) and B3LYP (OsB_2) in Molpro 2015.[1] The 3rd order DKH Hamiltonian was applied to Re and Os clusters. The VDEs were calculated by performing CASPT2 on the neutral. The aug-cc-pVQZ basis set was used on B and cc-pVTZ-DK3 was used for Re and Os. For TiB_2 clusters the cc-PVQZ clusters were used all around. We adopted this procedure because we have previously shown late transition metal borides are not well treated by DFT.[2] For alternate minima and all calculated states see SI Tables 1-5. NBO charges and DFT energies were obtained with Gaussian09 and lanl2dz basis sets with the PBEPBE functional.[3] To determine the bonding and antibonding character in the solids, a COHP analysis was run using the LOBSTER software.[4]

All solid-state calculations were carried out in VASP with PBE.[5] For Bader charges the OsB_2 and ReB_2 structures used a 15x19x15 k-mesh, and the TiB_2 structure used a 17x17x17 k-mesh.

b. Experimental Methods

Anion photoelectron spectroscopy is conducted by crossing a beam of mass-selected negative ions with a fixed-frequency photon beam and energy-analyzing the resultant photodetached electrons. The photodetachment process is governed by the energy-conserving relationship: $h\nu = EBE + EKE$, where $h\nu$ is the photon energy, EBE is the electron binding energy, and EKE is the electron kinetic energy. Our apparatus consists of a laser vaporization cluster anion source, a time-of-flight mass spectrometer, a Nd:YAG photodetachment laser, and a magnetic bottle electron energy analyzer.[6,7] The photoelectron spectrometer resolution is ~35 meV at 1 eV EKE. The third (355 nm) harmonic output of a Nd:YAG laser was used to photodetach electrons from mass-selected ReB_2^- and TiB_2^- clusters. Photoelectron spectra were calibrated against the well-known atomic transitions of atomic Cu^-.[8] The ReB_2^- and TiB_2^- anions were generated in a laser vaporization ion source. It consisted of either a rotating, translating rhenium boride rod or a titanium boride-coated copper rod, which were ablated with second harmonic (532 nm) photon pulses from a Nd:YAG laser and expanded with 80 psi of helium gas.

The powder (around 10 grams) was packed into a long balloon and placed under vacuum to remove any air bubbles that might have gotten into it. This was then tied up and placed in a hydrostatic press and placed under 70 MPa for 10 minutes. It was carefully removed and the balloon was cut. The rod (0.635cm diameter x 6.5cm length) was then carefully placed in an alumina boat and fired under argon gas at 1000 C overnight. The rod was firm and strong the next day.

2. Results and Discussion

a. Experimental and Simulated Mass Spectra of ReB_2^- and TiB_2^-

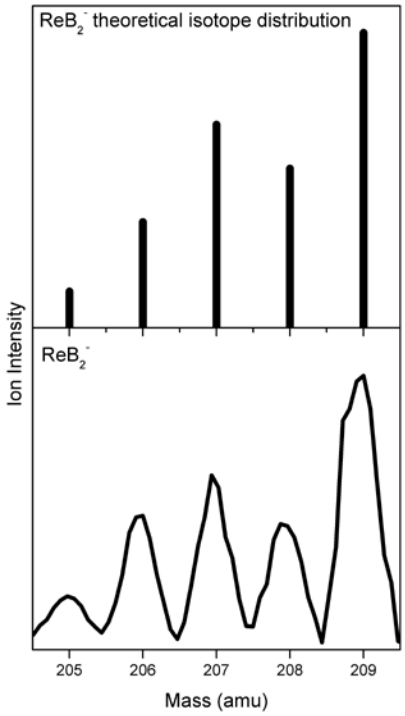

Figure S1. Experimental and simulated mass spectra of ReB_2^-.

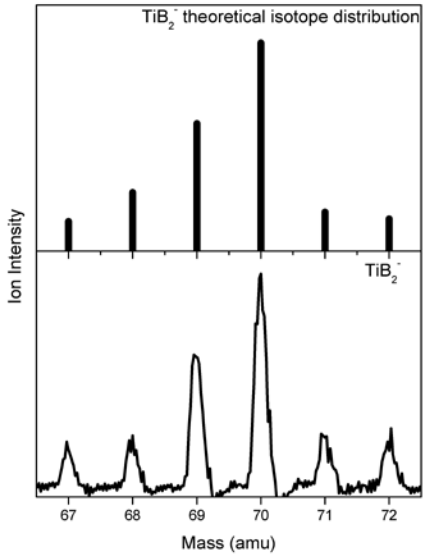

Figure S2. Experimental and simulated mass spectra of TiB_2^-.

b. Alternate Minima and Excited States of Clusters

Table S1. CASPT2 Geometry optimizations of the low-lying states of neutral and anionic ReB_2. The CASPT2 gradients were based on a CASSCF(9,11) and CASSCF(10,11) for the neutral and anion respectively. To assure that intruder states were not an issue, a level shift of 0.2 was applied to all CASPT2 calculations.

Species	State	Re(η^2-B_2) (Å)	B-B length (Å)	□E (eV)
ReB_2^-	$^3A_1$	1.76	1.66	0.428
ReB_2^-	$^3B_1$	1.72	1.66	0.116
ReB_2^-	$^3B_2$	1.66	1.75	0.000
ReB_2^-	$^3A_2$	1.71	1.76	0.136
ReB_2	$^4B_1$	1.73	1.65	0.000
ReB_2	$^2B_1$	1.74	1.66	0.191
ReB_2	$^4B_2$	1.56	1.99	0.851
ReB_2	$^2B_2$	1.59	1.89	0.804

Table S2. B3LYP Geometry optimizations of the low-lying states of neutral and anionic ReB_2. The results are within 0.02 Å of the CASPT2 opt, so this method was used for OsB_2.

Species	State	Re(η^2-B_2) (Å)	B-B length (Å)
ReB_2^-	$^3B_2$	1.68	1.70
ReB_2	$^4B_2$	1.54	2.01
ReB_2	$^2B_2$	1.75	1.60

Table S3. Calculated vertical detachment spectrum of ReB_2 isomers. The fluxionally of the bond length and the near degeneracy of several states makes assigning transitions impossible. The spectrum is calculated by subtracting the anion energy and the neutral energy.

	Anion $^3B_2$ Geometry		Anion $^3A_2$ Geometry		Anion $^3B_1$ Geometry	
State	□E (eV)	VDE (eV)	□E (eV)	VDE (eV)	□E (eV)	VDE (eV)
$^4B_1$	0.000	1.76	0.000	1.58	0.000	1.51
$^2B_1$	0.203	1.96	0.188	1.77	0.195	1.70
$^2A_1$	0.520	2.28	0.641	2.22	0.617	2.13
$^2B_2$	0.784	2.55	0.816	2.40	0.888	2.40
$^4B_2$	0.927	2.69	1.069	2.65	1.305	2.81
$^4A_2$	1.222	2.98	1.221	2.80	1.429	2.94
$^2A_2$	1.270	3.03	1.254	2.84	1.560	3.07
$^4A_1$	1.780	3.54	1.756	3.34	1.880	3.39

Table S4. B3LYP Geometry optimizations and DFT energies of the low-lying states of neutral and anionic OsB_2.

Species	State	Os(□^{2}-B_2) (Å)	B-B length (Å)	□E (eV)
OsB_2^-	$^4A_2$	1.68	1.66	0.000
OsB_2^-	$^6A_2$	1.87	1.57	1.361
OsB_2	$^3A_2$	1.60	1.91	1.796

OsB_2	$^5A_2$	1.58	1.93	2.993

Table S5. MRCI (CASSCF(10,10)) Geometry optimizations of the TiB_2 neutral and anion.

Species	State	Ti(□-B_2) (Å)	B-B length (Å)
TiB_2^-	$^2A_1$	1.98	1.56
TiB_2	$^1A_1$	1.84	1.54

c. Elastic Moduli of Structures

	Os Boat	Re Boat	Os Chair	Re Chair
Bulk Modulus Voigt Average (GPa)	323	341	350	357
Bulk Modulus Reuss Average (GPa)	318	333	322	347
Bulk Modulus VRH Average (GPa)	321	337	336	352
Shear Modulus Voight Average (GPa)	184	250	194	282
Shear Modulus Reuss Average (GPa)	148	238	180	270
Shear Modulus VRH Average (GPa)	166	244	187	276

Table S6. Calculated Shear, and Bulk moduli for all structures presented in text.

d. Elastic Tenors of Structures

	XX	YY	ZZ	XY	YZ	ZX
XX	578	181	189	0	0	0
YY	181	550	133	0	0	0
ZZ	189	133	775	0	0	0
XY	0	0	0	190	0	0
YZ	0	0	0	0	69	0
ZX	0	0	0	0	0	196

Table S7. Calculated elastic tensor (GPa) of Os Boat. (natural OsB_2 structure)

	XX	YY	ZZ	XY	YZ	ZX
XX	595	198	177	0	0	0
YY	198	589	115	0	0	0
ZZ	177	115	908	0	0	0
XY	0	0	0	226	0	0
YZ	0	0	0	0	197	0
ZX	0	0	0	0	0	293

Table S8. Calculated elastic tensor (GPa) of Re Boat.

	XX	YY	ZZ	XY	YZ	ZX
XX	480	200	218	0	0	0
YY	200	480	218	0	0	0
ZZ	218	218	913	0	0	0
XY	0	0	0	140	0	0
YZ	0	0	0	0	209	0
ZX	0	0	0	0	0	209

Table S9. Calculated elastic tensor (GPa) of Os Chair.

	XX	YY	ZZ	XY	YZ	ZX
XX	650	185	125	0	0	0
YY	185	650	125	0	0	0
ZZ	125	125	1048	0	0	0
XY	0	0	0	232	0	0
YZ	0	0	0	0	270	0
ZX	0	0	0	0	0	270

Table S10. Calculated elastic tensor (GPa) of Re Chair. (natural ReB_2 structure)

	XX	YY	ZZ	XY	YZ	ZX
XX	642	75	106	0	0	0
YY	75	642	106	0	0	0
ZZ	106	106	443	0	0	0
XY	0	0	0	258	0	0
YZ	0	0	0	0	258	0
ZX	0	0	0	0	0	283

Table S11. Elastic tensor (GPa) of TiB_2. Acquired from the materials project database.[9]

e. COHP Analysis

A Crystal Orbital Hamiltonian Population (COHP) analysis[10-12] was performed on ReB_2, OsB_2, and TiB_2 (see Figures S3 S4 and S5). COHP projects the plane wave solution onto a localized basis and uses that information to determine pairwise interactions between atoms in the solid producing a density of states plot, where a negative COHP value indicates bonding interactions and a positive COHP value indicates antibonding. Furthermore by integrating the COHP from infinity to the Fermi level (ICOHP) we can define specific bond energy. For a complete description of the COHP method and its implementation we refer the reader to reference 4.

Our COHP results confirm the ionic character of TiB_2 with the B-B bonds having a strength 8x greater than the incidental Ti-B bonds. In addition, COHP demonstrates that in both ReB_2 and OsB_2 there are significant bonding M-B (M=Re or Os) interactions. In fact, a

only negligible amount of antibonding character enters the valence space in the 2.15 Å Os-B bond while all the other bonds are entirely bonding. Looking at the ICOHP values, the 2.15 Å Os-B bonds have larger bond strengths than the 1.90 Å B-B bonds. This stands in contrast to ReB_2 where the B-B bonds are almost triple the strength of any Re-B interactions. (Fig S4). These bond strengths are consistent with the electron density values from our QTAIM analysis (see main text).

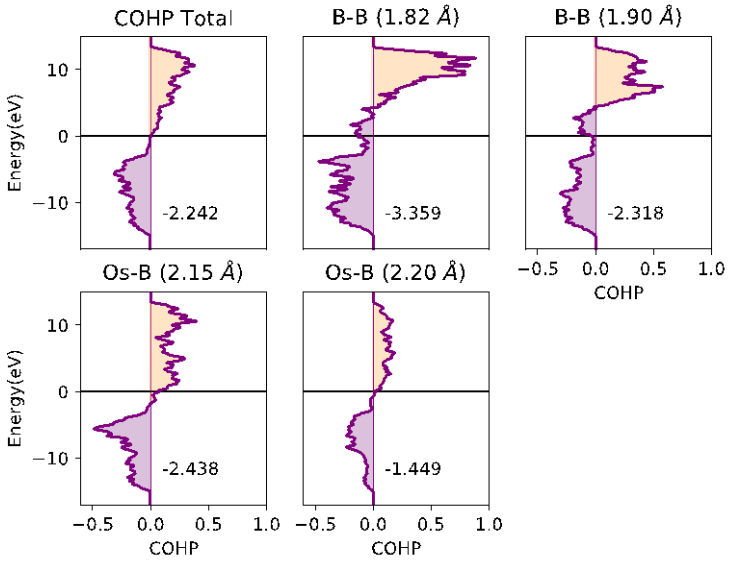

Figure S3: COHP analysis of OsB_2 both as a whole (top left) and broken down bond by bond. The ICOHP values (bottom right of each figure) confirm that the Os-B interactions in the solid are stronger than some of the B-B interactions.

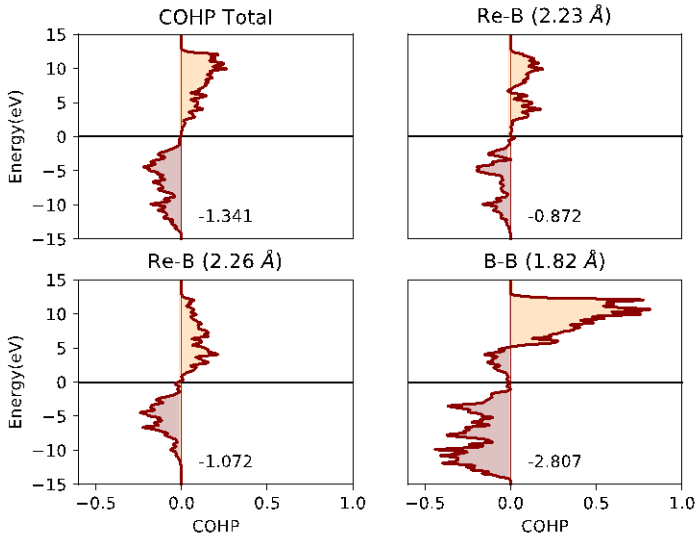

Figure S4: COHP analysis of ReB_2 both as a whole (top left) and broken down bond by bond. The ICOHP values (lower right of each plot) show that the B-B interactions are much stronger than the Re-B interactions.

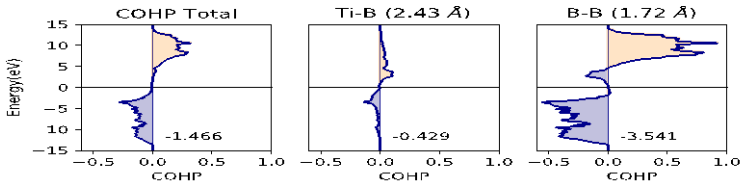

Figure S5: COHP analysis of TiB_2 both as a whole (left) and broken down bond by bond. The ICOHP values (lower right of each plot) show that the B-B bonds are more than 8x stronger than the Ti-B bonds**.**

References

(1) H. -J. Werner, et al., *Wiley Interdiscip. Rev Comput. Mol. Sci.* **2012**, 2, 242-253.
(2) P. J. Robinson, X. Zhang, T. McQueen, K. H. Bowen, A. N. Alexandrova, *J. Phys. Chem. A* **2017,** 121,1849-1854.
(3) M. J. Frisch et al, Gaussian, Inc., Wallingford, CT, USA, **2009**.
(4) R. Dronskowski, P. E. Blöchl, J. Phys. Chem. **1993**, 97, 8617–8624
(5) J. Hafner, *J. Comput. Chem.* **2008**, *29*, 2044-2078.
(6) X. Zhang, G. Liu, G. Ganteför, K. H. Bowen, A. N. Alexandrova, *J. Phys. Chem. Lett.* **2014**, 5, 1596-1601
(7) X. Zhang, P. Robinson, G. Gantefor, A. Alexandrova, K. Bowen, *J. Chem. Phys.* **2015**, *143*.
(8) H. Joe, K. M. Ervin, W. C. Lineberger, *J. Chem. Phys.* **1990**, *93*, 6987.
(9) M. De Jong, W. Chen, T. Angsten, A. Jain, R. Notestine, A. Gamst, M. Sluiter, C.K. Ande, S. Van Der Zwaag, J.J. Plata, C. Toher, *Scientific data*, **2015**, *2*, 150009
(10) V. L. Deringer, A. L. Tchougréeff, R. Dronskowski, J. Phys. Chem. A **2011**, 115, 5461–5466
(11) S. Maintz, V. L. Deringer, A. L. Tchougréeff, R. Dronskowski, J. Comput. Chem. **2013**, 34, 2557–2567
(12) S. Maintz, V. L. Deringer, A. L. Tchougréeff, R. Dronskowski, J. Comput. Chem. **2016**, 37, 1030–1035.